Simulating multimode DFB laser chaotic emission with a filtered unidirectional nonlinear loop mirror

M. FADHALA*, S. KHORSHEED*
Department of Physics, College of Sciences, University of Al-Nahrain, Baghdad, Iraq

In this simulation study, unidirectional optical loop-mirror type is simulated by using an optical fiber. The laser source that feeds the loop mirror is a multimode distributed-feedback laser (DFB). Optisystem 18 software was used to configure the setup, which included four laser sources. Effect of amplifier gain on a circulated chaotic signal within the loop mirror in addition to filtering. Results indicated that amplificating with 20, 50, and 80 dB values the circulated optical feedback and injection inside the filtered loop mirror gives rise to chaotic dynamics in both single mode and multi-mode lasers. Broadening and annihilation of lasing frequencies are observed in the resulting power and RF spectra. The input optical power 0.878 after amplifier become 6.939 dB, while -17.369 to 43.610 dB at Gain of optical amplifier 80 dB. The optical spectrum becomes sharper than that observed in the free-running identical spectrum. It is expected that with operation, the two modes will be enhanced due to the filtering associated with the reflected portion, compared with the spectrum associated with the transmitted spectrum. There was a new, lower-amplitude mode that accompanied each mode. We shall use the term “coherence collapse” in this paper exclusively to describe the optical injection catastrophic line broadening in a DFB. The chaotic signal follows steps before becoming similar to the coherent collapse effect. This will be a new result in simulating coherence collapses. It employs an interferometer to enhance encryption via chaotic signals. Increasing security in this experiment is based on different mechanisms that improve security. In addation that, tested parameters such as phase, amplification, filtration, and current operation level were added to the chaotic dynamics introduced in this work.

(Received October 13, 2023; accepted June 5, 2024)

Keywords: Chaos, FBG Sensor, Distributed-Feedback Laser, Nonlinear Optical Loop Mirror, Gain, Multimode

1. Introduction

The nonlinear-optical loop mirror for ultrafast processes was first proposed and analyzed by Doran *et al.* in 1988. All-optical switching geometry was demonstrated and studied with reference to erbium doped fiber amplifier EDFA and nonlinear loop mirror combination. These devices are based on the nonlinear property of a fiber loop formed by connecting the output parts of an interferometer coupler [1]. Optical fibers attenuate light like any other material. In the case of silica fibers, losses are relatively small, especially in the wavelength region near 1.55 μm ($\alpha \approx 0.2$ dB/km). For this reason, losses can simply be ignored if the fiber length is 1 km or less [2]. Optoelectronic repeaters, in which the optical signal is first transformed into an electric current and then regenerated using a transmitter, have historically been used for long-haul systems to bypass the loss restriction. In wavelength-division multiplexed lightwave systems, such regenerators become highly sophisticated and costly. Using optical amplifiers, which directly amplify the optical signal without necessitating its conversion to the electric domain, is an alternate method of loss management [3]. High power lasers are needed for most of these applications. The master oscillator power amplifier technique is one way to reach the high powers [4]. When it comes to modern fiber-optic communication systems, EDFAs have garnered the most attention because they operate near 1.55 μm and are useful for overcoming transmission losses and restoring the optical signal. Amplifier characteristics, such as the operating wavelength and the gain bandwidth, are determined by dopants rather than by the fiber, which acts as a host medium [2].

In light-wave communication systems, EDFA is important. Attenuation losses within the fiber must be compensated for in order to send messages across long distances (>100 km), as the combined effects of dispersion and attenuation cause the signals to become weaker, indiscriminate, and more difficult to detect [5]. Fiber Bragg gratings, or FBGs, are a type of structure that function as a narrowband reflected spectral filter in astronomy. They have a refractive index modulation. Specifically, FBGs are employed as cavity mirrors in doped fiber-based lasers as EDFAs with broad gain profiles [6] [7]. It is anticipated that the optical fiber's transmission capacity will be used more effectively, and that signal-processing equipment will likely be simpler and less costly. Devices that use light to control light signals in particular hold great promise since control and data signals can both be sent through the same optical fiber. The nonlinear optical loop mirror (NOLM), also known as the nonlinear Sagnac interferometer, is one such instrument. Two significant characteristics of the NOLM are its intrinsically rapid response time, which is based on fiber nonlinearity and allows for ultrafast data processing, and the intrinsic stability of its interferometer structure. Large optical powers and lengthy fiber lengths are necessary for the NOLM, though. Sagnac interferometer

principle as the NOLM. Nevertheless, the erbium doped fiber amplifier in the loop and optical injection, rather than the optical nonlinearity of the fiber, are what drive its operation [7].

First, a period-doubling pathway to optical chaos was found to be triggered by a ring resonator's nonlinear response. Every round trip's evolution of the intracavity field A(z; t) is controlled by the standard nonlinear Schrodinger equation. [2]:

$$i\frac{\partial A}{\partial z} - \frac{\beta_2}{2}\frac{\partial^2 A}{\partial T^2} + \gamma|A|^2 A = 0 \quad (1)$$

where $T = t - z/v_g$ the reduced time and β_2 is the group velocity dispertion parameter.

An innovative use of nonlinear dynamics in the chaotic regime, chaos-based encryption first surfaced in the early 1990s and has since become a significant topic in optical communications. Chua's circuit produced the first experimental realizations in electronics, but because optics is a field that studies nonlinear phenomena, the optics community quickly expressed considerable interest in this new scientific application [8].

The EDFA is a tool that may be used to shape and enhance contrast of optical pulses as a nonlinear gain element [7]. The propagation equation, which is expressed in terms of the parameter needed in each chosen mode, relates the input data. Gain control, power control, and saturation control are the three distinct modes of operation [9]. The propagation and rate equations of a homogeneous, three-level laser system-the foundation of a 980 nm pumped EDFA-are used to model them. Considering the level 3, system [10], R is the pumping rate (or absorption rate) from level 1 to level 3, or 980 nm of pumping. W_{12} and W_{21} are absorption rate and stimulated emission rate between level 1 & 2, A_{21} is a spontaneous decay rate from level 2 to level 1. A is the non-radiative decay rate from level 3 to level 2. These three level laser system definitions are; level 1 is the ground level, level 2 is the metastable state having a life time $\tau = 1/A_{21}$ and level 3 is the pump level. Then the atomic laser rate equations of these three levels can be written as [10] [11];

$$\frac{dN_1}{dt} = -RN_1 - W_{12}N_1 + W_{21}N_2 + A_{21}N_2 \quad (2)$$

$$\frac{dN_2}{dt} = W_{12}N_1 - W_{21}N_2 - A_{21}N_2 + A_{32}N_3 \quad (3)$$

$$\frac{dN_3}{dt} = RN_1 - A_{32}N_3 = 0 \quad (4)$$

where N_1, N_2 and N_3 are the electron densities in levels 1,2 & 3. By considering the fact that $A_{32} >> R$ populations of the three level systems are [11];

$$N_1 = \rho\frac{1+W_{21}\tau}{1+(R+W_{12}+W_{21})\tau} \quad (5)$$

$$N_2 = \rho\frac{(R+W_{12})\tau}{1+(R+W_{12}+W_{21})\tau} \quad (6)$$

$$N_3 = \frac{R}{A_{32}}n_1 \approx 0 \quad (7)$$

where $\rho = N_1 + N_2 + N_3$ is the erbium ion concentration. As shown in equation, N_3 is zero [13], this is due to the fast decay from level 3 to 2. Therefore, 980 nm pumped EDFA can be analyzed by considering only levels 1 & 2 [10].

2. Theory

Three operation modes are enabled by the Flat Gain EDFA subsystem, and you can choose one by clicking on main/operation mode/value in the software menu to open the Flat Gain EDFA properties dialog box. The gain control option is the first one; it keeps the gain constant and lets you decide whether to include enhanced spontaneous emission in the calculations or not. The output power is continuously maintained in the second operation mode option, power control. The amplifier is considered to be in a saturated state in the third operation mode, saturation, when it is running at an output signal power that corresponds to a gain that is 3 dB less than the saturated gain. [13]. In gain control mode, you set the desired amplifier gain (in dB units), which is given by the ratio of the total output power (Pout) and total input power (Psin), including (or not including) the generated Amplified Spontaneous Emission (ASE), so the power (P_{ASE}), as given by [3]:

$$G = \frac{P_{out} - P_{sin}}{P_{ASE}} \quad (8)$$

This mode does not require any further iterations or complex equation solutions. The performance of this sub-system to be introduced into the global system is determined by the established amplifier input parameters, such as gain and noise figure. The desired amplifier output power (in dBm units) is the value you define in the power control mode, and it is continuously maintained. The amplifier will saturate and the maximum power will be decided by the input power amplified by the parameter gain if the gain needed to maintain the target output power is greater than the value of the gain parameter. The designed amplifier does not require any extra computation, much like the gain-controlled mode. The amplifier's performance is defined by the output power supplied as an input parameter. It should be noted that the ASE noise present in the amplifier subsystems does not reduce the stated output power; rather, the global system analysis computes this noise source. The input noise will not be included in the computed input power when using the signal power control mode [13].

The amplifier operates in a saturated regime when it is in the saturation mode, which is predicated on the pump power being constant. This mode requires three parameters: the noise figure, gain, and saturation power. The saturation power is the input parameter maintained constant in this mode selection, and in an ASE-free model

can be related with the gain (G), output power (P_{out}), and intrinsic saturation power (P_{sat}^{int}) by the expression [3]:

$$G = G_{\circ} exp\left[-\frac{G-1}{G}\frac{P_{out}}{P_{sat}^{int}}\right] \quad (9)$$

where G_0 is the small-signal gain or unsaturated gain.

The intrinsic saturation power is written as [3]:

$$P_{sat}^{int} = \frac{Ahv}{\sigma_a \tau} \quad (10)$$

where A is the mode-field area, h is the Planck's constant, ν is the frequency at the propagating signal, σ_a is the absorption cross-section, and t is the τ metastable lifetime in silica. Since the intrinsic saturation power and the amplifier saturation power under gain compression conditions are related, these fiber requirements are not necessary for this amplifier module. The output power is proportionate to the intrinsic saturation power under the 3-dB gain compression. This relation is [13]:

$$P_{out}|_{coppressed}^{3dB} = ln(2)\, P_{sat}^{int} \quad (11)$$

When an EDFA is driven sufficiently hard into saturation the output power tends toward a limiting value (P_{sat}^{int}) which is the maximum output power. Saturated output increases approximately linearly with pump power. An increasing percentage of the pump light is converted to signal as the EDFA reaches deeper saturation. EDFAs are substantially saturated when used as boosters or power amplifiers to produce high output power [14].

Fiber amplifiers use the same technique that lasers use to enhance incident light: stimulated emission. An optical amplifier is, in fact, nothing more than a laser without feedback. Its primary component is the optical gain determined as [15]:

$$g = \sigma (N_1 - N_2) \quad (12)$$

where σ is the transition cross section and N_1 and N_2 are atomic densities in the two energy states.

Using the relevant rate equations, the gain coefficient g can be computed for both the three- and four-level pumping schemes. A homogeneously expanded gain medium's gain coefficient can be expressed as [2]:

$$g(\omega) = \frac{g_{\circ}}{1+(\omega-\omega_a)^2 T_2^2 + P/P_S} \quad (13)$$

where $g_{\circ}$ is the peak value, ω is the frequency of the incident signal, ω_a is the atomic transition frequency, and P is the optical power of the continuous wave (CW) signal being amplified.

The saturation power P_s depends on dopant parameters such as the fluorescence time T_1 and the transition cross section σ. The parameter T_2 in last equation is known as the dipole relaxation time and is typically quite small (0:1 ps) for fiber amplifiers. The fluorescence time T_1 varies in the range from 0.1 μs to 10 ms, depending on the dopant. Equation (12) can be used to discuss the important characteristics of optical amplifiers such as gain bandwidth, amplification factor, and output saturation power. We begin by considering the case in which $P/P_S \ll 1$ throughout the amplifier. This is referred to as the unsaturated regime since the gain remains unsaturated during amplification [3]. The difference becomes clear when one considers the amplification factor defined as [16]:

$$G = \frac{Pout}{Pin} \quad (14)$$

where P_{in} and P_{out} are the input and output powers of the CW signal being amplified. The amplification factor is obtained by solving [3]:

$$\frac{dP}{dz} = g(\omega)P(z) \quad (15)$$

where P(z) is the optical power at a distance z from the input end of the amplifier.

A straightforward integration with the conditions P (0) = P_{in} and P(L) = P_{out} shows that the amplification factor for an amplifier of length L is given by [16]:

$$G(\omega) = \exp\left(\int_0^L g(\omega)dz\right) = exp[g(\omega)L] \quad (16)$$

where g is assumed to be constant along the amplifier length. Both $G(\omega)$ and $g(\omega)$ are maximum at $\omega = \omega_a$ and decrease when $\omega \neq \omega_a$ [2]. The typical gain profiles for various optical amplifier types based around the 1.3 and 1.5 μm wavelength regions. Wide spectral bandwidths are seen to be provided by the Raman fiber amplifier, the erbium-doped fiber amplifier (EDFA), and the semiconductor optical amplifier (SOA). For this reason, wavelength division multiplexing applications are well suited for these sorts of optical amplifiers. In contrast, the Brillouin fiber amplifier is not suitable for wideband amplification due to its extremely small spectral bandwidth, which may be as little as 50 MHz [17].

On the one hand, depending on whether the injection is unidirectional or mutual, optical injection can improve the line shape function for the Fourier spectrum to the injected laser [18] in additional to any optoelectronic feedback [19]. According to feedback type and purity, it can be making lasing tuned between more than one frequency [20] or even lead to hyper chaos spectrum [21]. The current study's goal is to examine the chaotic dynamics that arise when laser signals are amplified and travel through a nonlinear loop mirror after a particular filter is inserted to enable the splitting of light waves into two portions. In the event of optical injection, the impact of amplifier gain on the circulated signal is monitored and recorded. Making the feedback frequency-dependent so that the cavity loss varies for various longitudinal modes is one method of enhancing the mode selectivity. In this regard, two methods that have been proven to be helpful are referred to as coupled-cavity mechanisms and distributed feedback (DFB) lasers, which are used as the

optical source in the current work. As the name suggests, the feedback required for the lasing action in a DFB laser is dispersed along the cavity length rather than localized at the cavity facets. This is accomplished by using a grating that has been etched to cause periodic variations in one layer's thickness along the cavity length, which participates in the heterostructure. Feedback is provided by the ensuing periodic disturbance of the refractive index through reverse Bragg scattering, it unites the waves that propagate forward and backward. The Bragg condition gives rise to the DFB mechanism's mode selectivity. Essentially, a Fabry Perot laser with a Bragg grating above the active layer makes up the DFB laser. The Bragg grating's parameters are available under the "Grating" tab [22].

The DFB is set up as shown in Fig. 1 when the quarter wave shift in the center is not enabled. In this instance, there will be two dominant modes at equal distances on either side of the Bragg wavelength (note that one of these modes will typically be more prominent due to defects in real DFB lasers). The laser is shown in Fig. 2 when the quarter wave shift at the center is activated; in this instance, there will be a single dominant mode that is precisely at the Bragg wavelength. The dynamics of the DFB laser can be modeled using two techniques: transmission line and spatially averaged multimode. The DFB Laser Properties dialog's "Main" tab's Laser model drop-down menu field provides access to these models. The parameters control how the multi-mode laser reacts to a current waveform I(t). The input electrical signal is subjected to scale factors, namely modulation peak current and bias current. The internal current I(t) for the laser source is given by:

$$I(t) = I_{DC} + I_{in}(t) \times I_{pk} \tag{17}$$

where $I_{in}(t)$ is the input signal current, I_{DC} is the parameter Bias Current and I_{Pk} is the parameter Modulation peak current. If the parameter Bias Current and Modulation peak current have zero values, the internal current is given by $I_{in}(t)$ only.

The modulation dynamics of the DFB laser are modeled by the multimode rate equations which describe the relation between the carrier density N(t), photon densities $S_i(t)$, and optical phases $\varphi_i(t)$:

$$\frac{dN(t)}{dt} = \frac{I(t)}{q.V} - \frac{N(t)}{\tau_n} - \sum_i \left[G_i.(N(t) - N_t).\frac{1}{(1+\sum_i \varepsilon.S_j(t))}.S_i(t) \right] \tag{18}$$

$$\frac{ds_i(t)}{dt} = G_i.(N(t) - N_t).\frac{1}{(1+\sum_i \varepsilon.S_j(t))}.S_i(t) - \left(\gamma_p.S_i(t)\right) + \frac{\Gamma\beta N(t)}{\tau_n} + K_c.S_{ext}(t) \tag{19}$$

$$\frac{d\emptyset_i(t)}{dt} = \frac{1}{2}.\alpha\left[\Gamma.G_i.(N(t) - N_t) - \gamma_p\right] \tag{20}$$

where the gain (G_i) and the chirp (Δu_f) for each mode I, are defined by:

$$G_i = v_g.\sigma_g.\frac{\Gamma}{(1+\left(\frac{2i(f_i - f_o}{\Delta f}\right)^2)} \tag{21}$$

If the "Lifetime" recombination model is chosen, then:
σ_g is the differential gain coefficient
v_g is the group velocity
f_i is the frequency of the laser mode i
f_o is the laser central frequency
Δf is the 3dB gain bandwidth
ε is the gain compression factor
N_t is the carrier density at transparency
β is the spontaneous emission factor
$\boldsymbol{\Gamma}$ is the mode confinement factor
V is the active layer volume
γ_p is the cavity loss
τ_n is the carrier lifetime
α is the line-width enhancement factor
$S_{ext}(t)$ is the optically injected signal
K_c is the photon density coupling factor for the injected optical signal

If the "Lifetime" recombination model is chosen, then:

$$\frac{1}{\tau_n} = A + B.N + C.N^2 \tag{22}$$

where A, B, and C are the recombination coefficients.

The geographical distribution of the field inside the cavity is not taken into account by the "spatially averaged" multimode model. The common multimode rate formulae are applied. It is unable to model effects like spatial hole burning because of its averaged nature. It does, however, compute more quickly than the transmission line model. With the following exceptions, the multimode rate equations for the DFB laser model are comparable to those for the "Spatially averaged" Fabry Perot model:

The modes are either the single mode at the Bragg wavelength of the quarter wave shifted laser or the two dominant modes of the non-quarter wave shifted laser. Ignoring all other modes in the system yields an approximation that is typically accurate. Effective reflectivity is used in place of mirror reflectivity and is dependent on the DFB structure's modes [23]. Coupled mode theory is used to calculate the DFB modes. This makes intuitive sense as the Bragg grating will result in wavelength-dependent backscattering. These modes are dependent upon the coupling strength (derived from the "Grating index difference"), cavity size, and real mirror reflectivity [23]. An effective photon lifetime, or cavity loss in this case, which is likewise mode dependent, takes the role of the photon lifetime. This allows one to determine the threshold current [24].

Note: In the final term of equation (18), the spontaneous emission rate, often known as Rsp, may be substituted for 1/2ρn on occasion. Both formats are fine, but it's crucial to choose the spontaneous emission factor

appropriately. There are several sections that make up the laser cavity. The nodes that allow the field (also known as "voltage") to disperse forward and backward connect the sections. Assuming a Lorentzian line-width, the differential gain, damping, 3dB frequency, and attenuation in the active layer are used to calculate the gain and loss of the field, which are modeled in the time domain. Additionally, the transmission-line modeling (TLM) approach is used to estimate the carrier rate equation. A stochastic voltage term is incorporated into each segment to simulate spontaneous emission. In order to model the DFB structure, each transmission line section is alternated between "high" and "low" impedances (the two center layers will have the same impedance for the quarter wave shift), which will produce matching scattering matrices at each node. Since some of the higher harmonics of these alternating impedance structures will correlate to the DFB modes, it can be demonstrated that this can represent the true DFB grating modes [25]. The model incorporates frequency chirping by connecting additional impedances to circulators [25]. Using the same coupling constant as the Spatially Average Multimode model, the injected field is added to the leftmost element at each time-point to accommodate external optical injection [26]. It is advised to use no more than 50 sections (according to the "Numerical" tab's "Number of cavity sections") for computational efficiency; if the findings are precise enough, using 20–30 sections is better. The field at the rightmost laser cavity X (1 - reflectivity) is the laser's output field. The Laser model drop-down menu field on the "Main" tab of the DFB Laser Properties dialog box allows users to access these models from the Optisystem program.

3. Simulation set-up

The schematic diagram for the setup is given in Fig. 1. It includes an EDFA with three gain scales (20, 50, and 80 dB). This amplifier is located inside a loop mirror and is forced to run unidirectionally. The original signal is received from a laser source whose type is a multimode DFB laser. With the same laser type, three additional laser sources are connected via optical fiber and radio frequency to measure the effect of perturbed signals on these lasers. The effect of optical amplification on nonlinearity generated via returned signals is observed. The laser is operated in a stable multi-wavelength condition at room temperature. The uniform fiber Bragg grating (UFBG) inside the loop provides wavelength-shifted feedback, which is filtered. The use of such a laser, especially multimode, is more attractive due to the capabilities offered by dual modes. A guided mode propagating in UFBG can be coupled to another propagating in the opposite direction to generate a narrow-band reflection, which is employed in this setup.

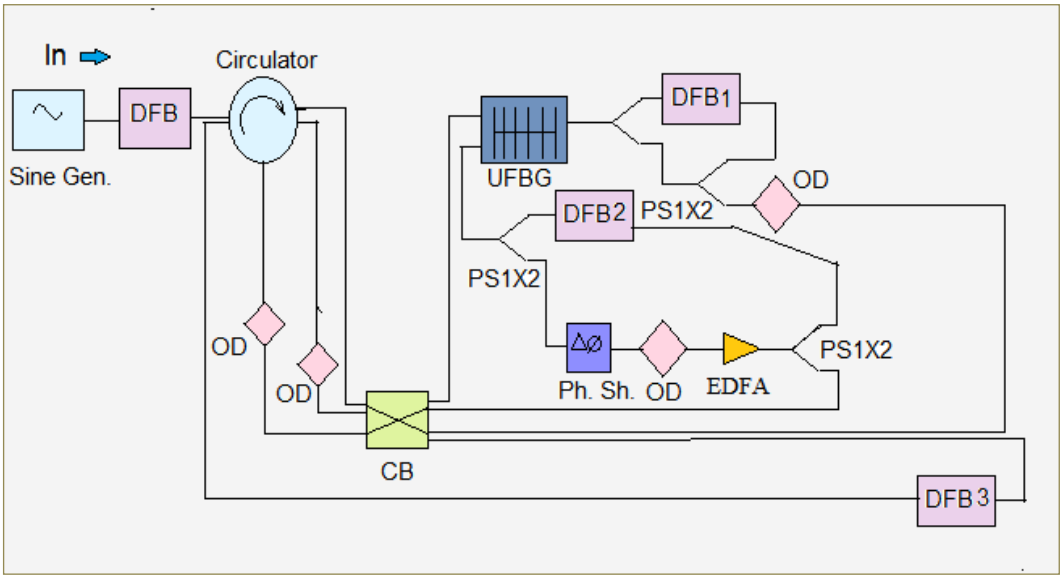

Fig. 1. Schematic diagram of experiment. Sine Gen. is a sine generator, DFB is a multimode laser source; DFB1, DFB2, and DFB3 are the lasers that receive the optical injection from the loop mirror, OD is the optical delay (delay =5), CB is the bidirectional coupler, Ph. Sh. is the phase shifter, and finally, PS12 is the power splitter (color online)

The exact setup is given in Fig. 2. A sine generator is used only to enable the laser source to run under program considerations. A fine selection for laser input power is done to select the values that are expected from the output side. With several inputs, lasers can give single modes, and with another's, multimode can result. Activation for multimode and canceling this operation type is possible in Optisystem by accessing the Laser model menu and selecting quarter wave shift at the center as "NO". The bias current is set to be equal to 27 mA after testing the threshold level for the laser in the free-running situation. The Bragg wavelength selection is 1550 nm to be compatible with long-haul optical fiber applications.

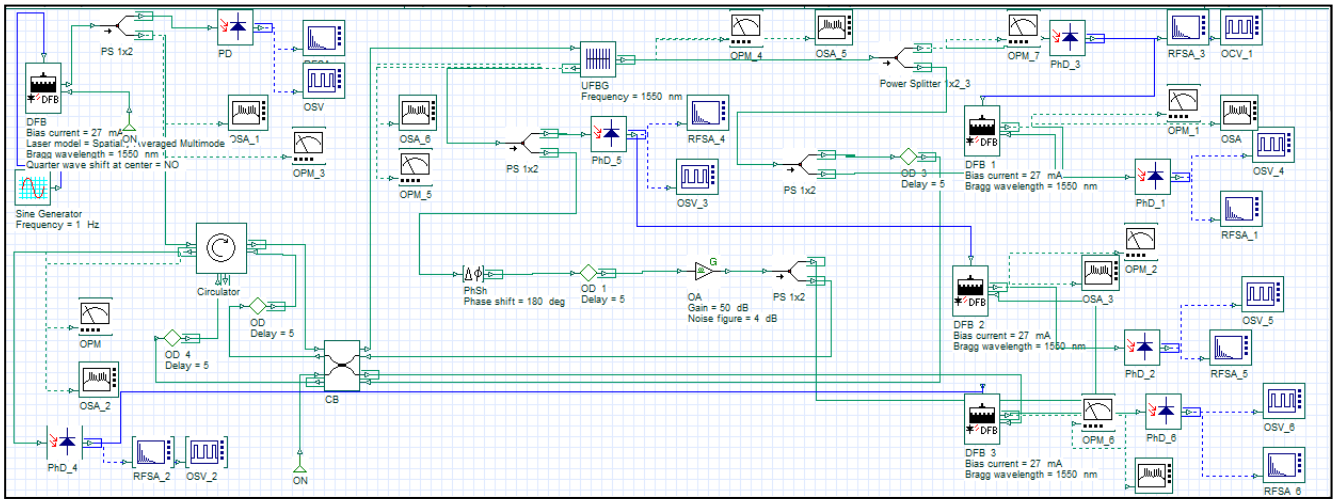

Fig. 2. Simulation setup for chaos by NOLM (color online)

In this scheme, the main ingredient is the optical gain realized when the amplifier is pumped (optically or electrically via bias) to make the medium achieve population inversion. As reported in [3] the optical gain, in general, depends not only on the frequency (or wavelength) of the incident signal, but also on the local beam intensity at any point inside the amplifier. Details of the frequency and intensity dependence of the optical gain depend on the amplifier medium.

4. Results and discussion

Signal strength inside the nonlinear optical loop mirror, the nonlinear Kerr effect, pump modulation, and loss modulation are the four main techniques for chaotic creation in EDFA. Ref. [26] employed, numerically, the NOLM as a quick-saturable absorber to Sagnac interferometers or passively mode-locked laser oscillators. Optical instabilities with optical injection demonstrated that the NOLM with optical injection can result in the period-doubling route to chaos. The measured input optical power (in dBm) (optical injection) and output power (in dBm) for different gain values of the optical amplifier (20, 50, and 80 dB) for unidirectional optical injection for four lasers (the first one in input and three lasers in output of the loop mirror) are given in Table 1.

The discussion of the results given in Table 1 can be interpreted by reference to equation (13), where the outpower increased with increased gain of EDFA. The phase shift is set at 180 degrees, frequency of sine generation is set at 1Hz and the wavelength is 1550 nm, while the operating temperature is stabilized at 20 °C. Additionally, variable optical delay lines are selected to temporally align the chaotic waveforms which is observed. The optical time delayed feedback is re-injected towards the DFB lasers outputs again which meets requirements mentioned in [8] and [27].

Table 1. Gain of OA data, input and output powers for DFB lasers used

Laser	Gain of OA (dB)	Input optical power (optical injection) (dBm)	Output power (dBm)
DFB	20	/	6.939
	50	/	6.942
	80	/	6.977
DFB1	20	0.878	7.064
	50	0.917	7.117
	80	0.976	7.169
DFB2	20	-17. 064	4.923
	50	-17. 164	14.287
	80	-17. 369	43.610
DFB3	20	-53.027	9.656
	50	-53.067	9.710
	80	-53.086	9.748

4.1. Input spectrum to NOLM

Fig. 3 shows the observed dynamics for the laser source just before entering the circuit. The performance of laser is measured by an optical spectrum analyzer, RF spectrum analyzer and oscilloscope visualizer. These dynamics are observed as multimode spectra without any external effect.

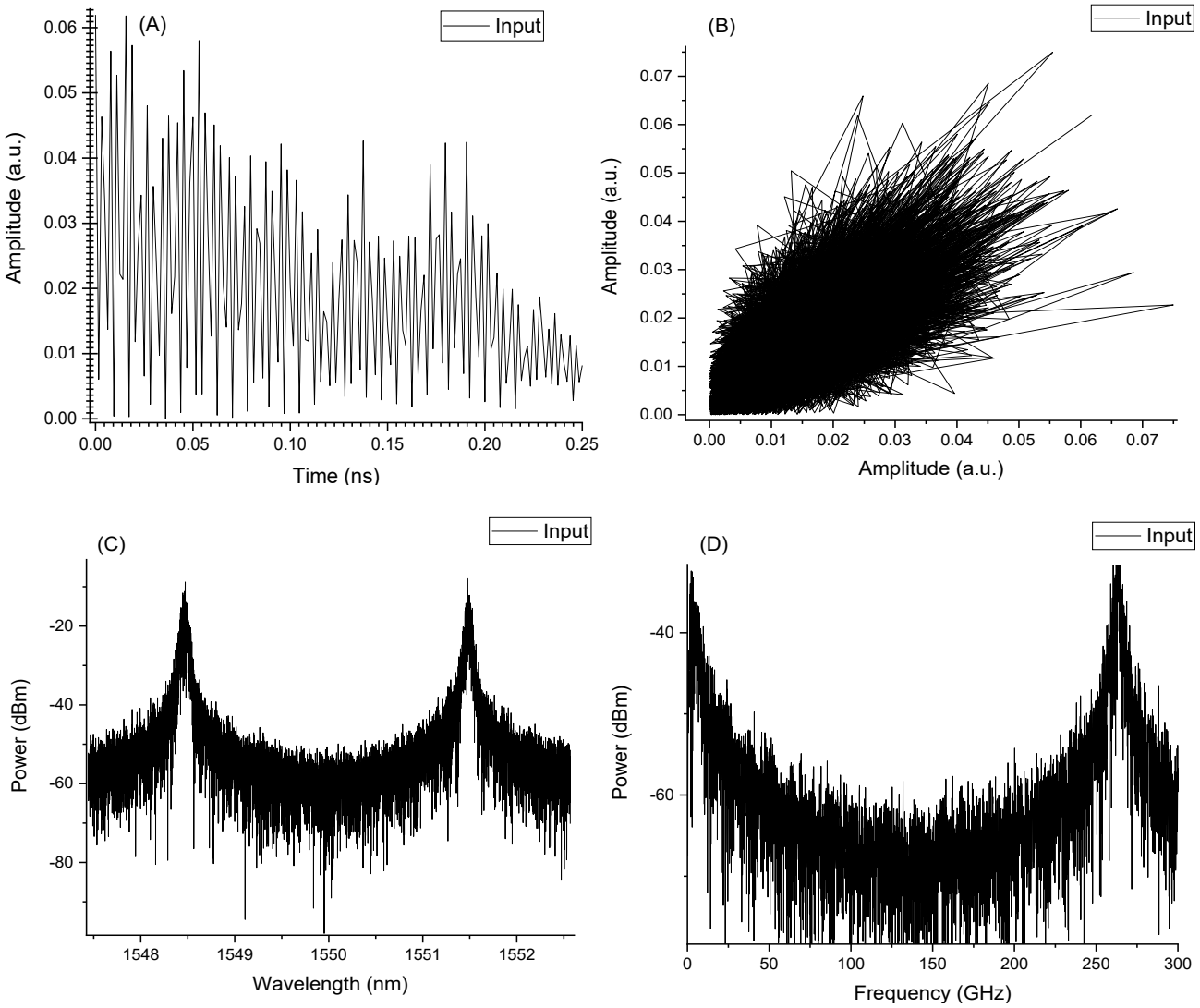

Fig. 3. Observed Dynamics for free running laser.
(A) Time series, (B) Phase space, (C) Optical spectrum and (D) Radio frequency spectrum

The input signal has the shape of CW before the injection inside the loop. It amplified when reflected from UFBG, i.e., for wavelets that satisfy the Bragg wavelength, then circulated into the loop after passing through the 1X2 splitter. One of the two arms undergoes a phase shift and optical delay, and then optical amplification is nonlinear process due to chaotic dynamics. The remaining arm will be detected and modulated into DFB2. The signal is collocated again by bidirectional coupler. From the same figure, both optical and frequency spectra indicate a two modes laser emission, given from last spectrum in two peaks; 1548.4 and 1551.5 nm.

Based on the observed diagnosed signal, all the coming measurements obtained on the signal with the option of "without noise" from the Optisystem menu (sampled signal), depending on reference [28].

4.2. Loop dynamics with 20dB Gain

EDFA is inserted inside the loop to introduce amplification and nonlinearity gain for the optical signal. Such a gain is provided in shape and contrast enhancement for the chaotic carrier as broadening in its bandwidth, which agrees with what is reported in Ref. [29]. In addition to that, unidirectional optical injection introduced more nonlinearity effects, which are used in different positions inside the NOLM for DFBs.

4.2.1. Multimode DFB1 laser

This laser source is inserted after an UFBG, and the transmitted spectrum from this filter becomes an input for it. The results shown in Fig. 4(C, D) indicate generation for new neighbor modes directly behind the original modes, with peak wavelengths of 1548.5, 1548.7, 1551.5, and 1551.75 nm. Based on the attractor, such new lasing peaks appeared, and the route to chaos states was observed.

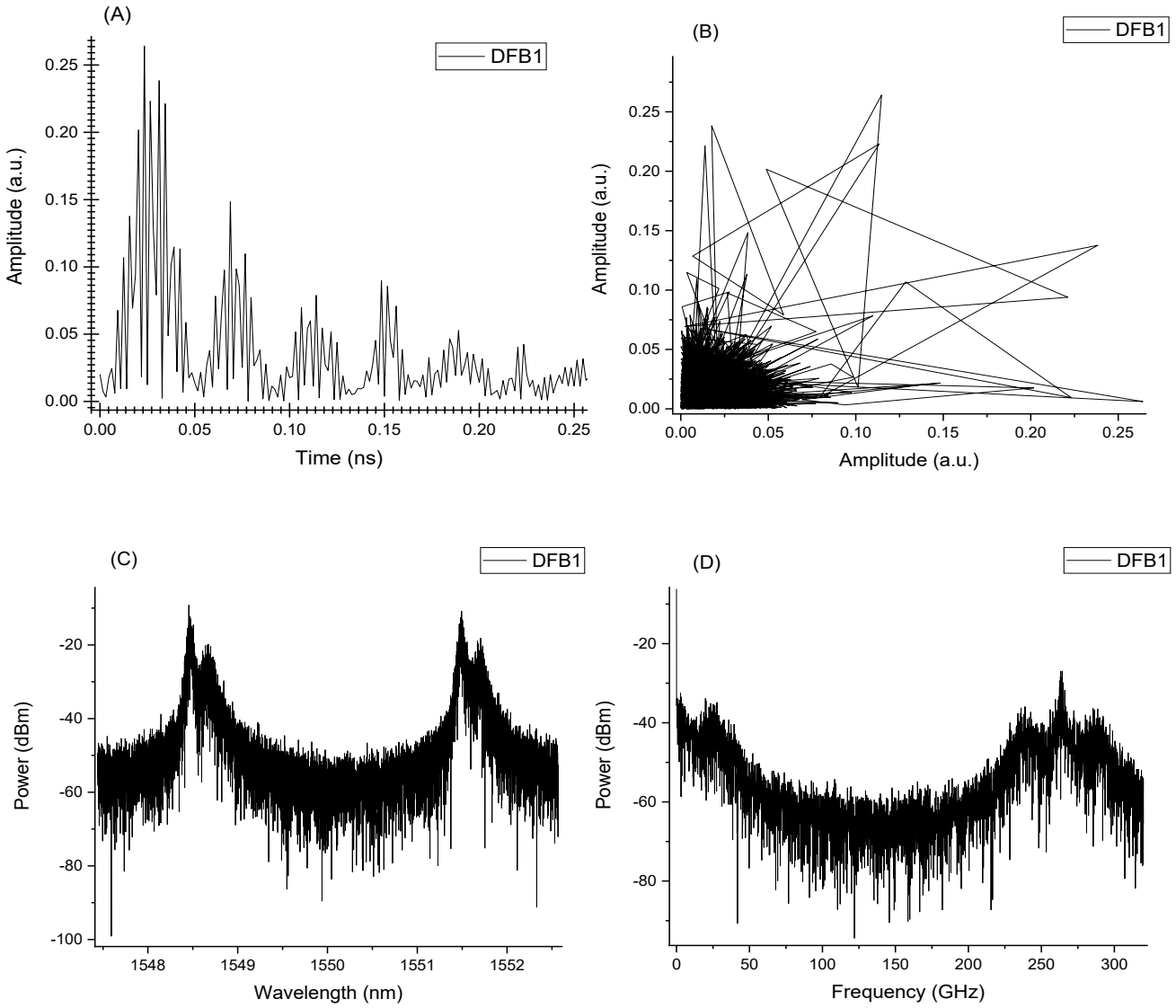

Fig. 4. Observed spectrum of DFB1 of 20 dB gain of EDFA.
(A) Time series, (B) Phase space, (C) Optical spectrum and (D) Radio frequency spectrum

There was a new, lower-amplitude mode that accompanied each mode. The chaotic signal follows steps before becoming similar to the coherent collapse effect. This will be a new result in simulating coherence collapses. Coherence collapse is always attributable to deterministic chaos. Most incidents of coherence collapse should therefore be due to quasiperiodic mixing between the relaxation oscillation and external cavity modes [30].

4.2.2. Multimode DFB2 laser

DFB2 is interested in the reflected port from the UFBG; this spectrum is the same as the input spectrum, but its wavelengths are red-shifted in Fig. 5C. The shifted wavelengths are 1548.64 nm and 1551.65 nm. The same shift is shown in the frequency spectrum in Fig. 5D. This indicates a modification in the semiconductor active medium inside this laser source. Spikes are observed in the resulting spectrum, with different spacing between them

indicating the interaction between different circulating modes.

The DFB2 optical spectrum becomes sharper than that observed in the free-running identical spectrum. It is expected that with this operation, the two modes will be enhanced due to the filtering associated with the reflected portion, compared with the spectrum associated with the transmitted spectrum.

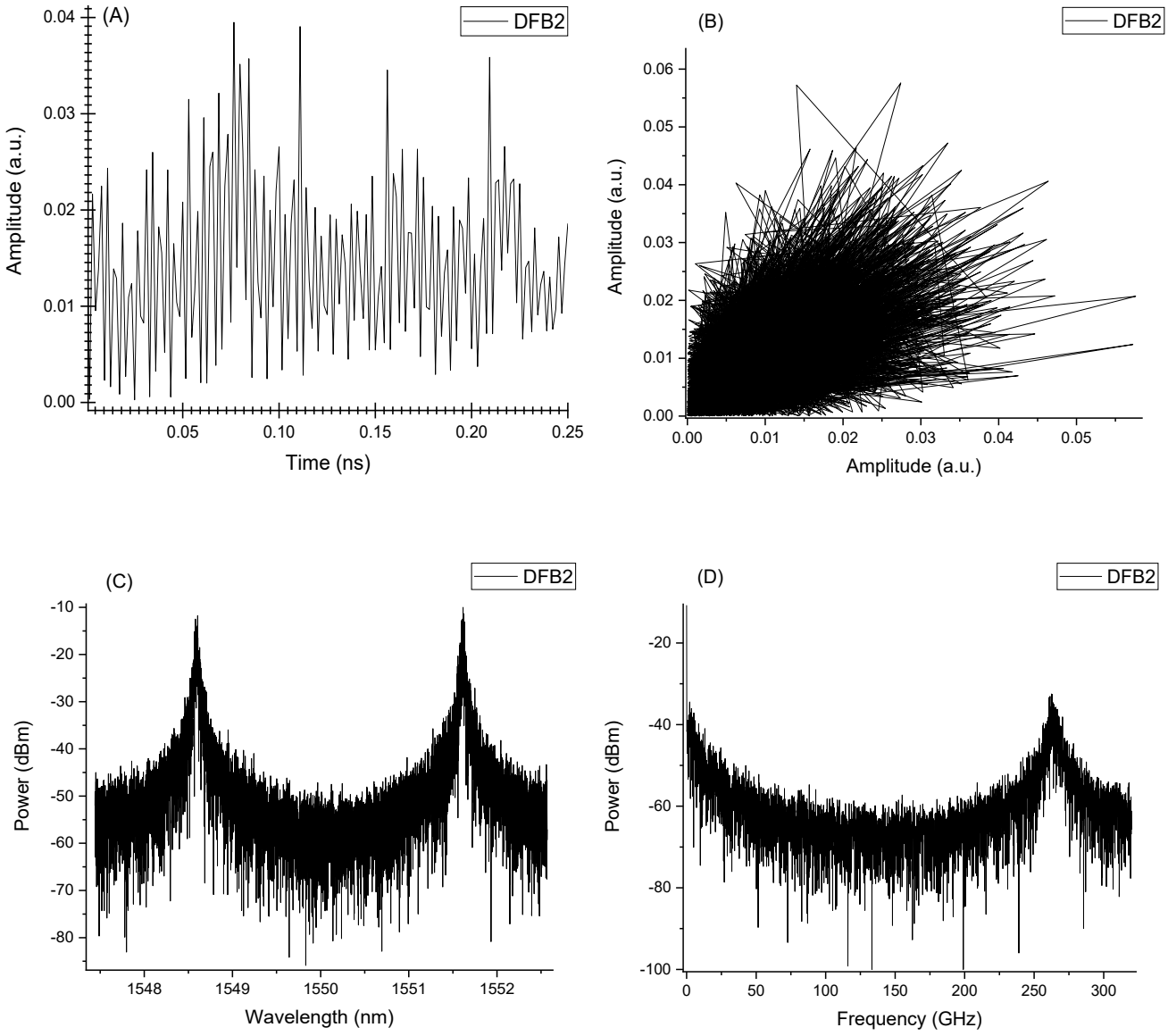

Fig. 5. Observed spectrum of DFB2 of 20 dB gain of EDFA.
(A) Time series, (B) Phase space, (C) Optical spectrum and (D) Radio frequency spectrum

4.2.3. Multimode DFB3 laser

DFB3 is inserted after the NOLM, which means the output of the loop become input of DFB3. The resulting spectrum is shown in Fig. 6. Several modes appeared more than those observed with DFB1, Fig. 4. A more complicated chaotic signal is resulted under the effect of an amplified circulated path inside the loop mirror. The observed wavelengths are 1548.5 nm, 1548.8 nm, and 1551.5 nm, 1551.85 nm.

.

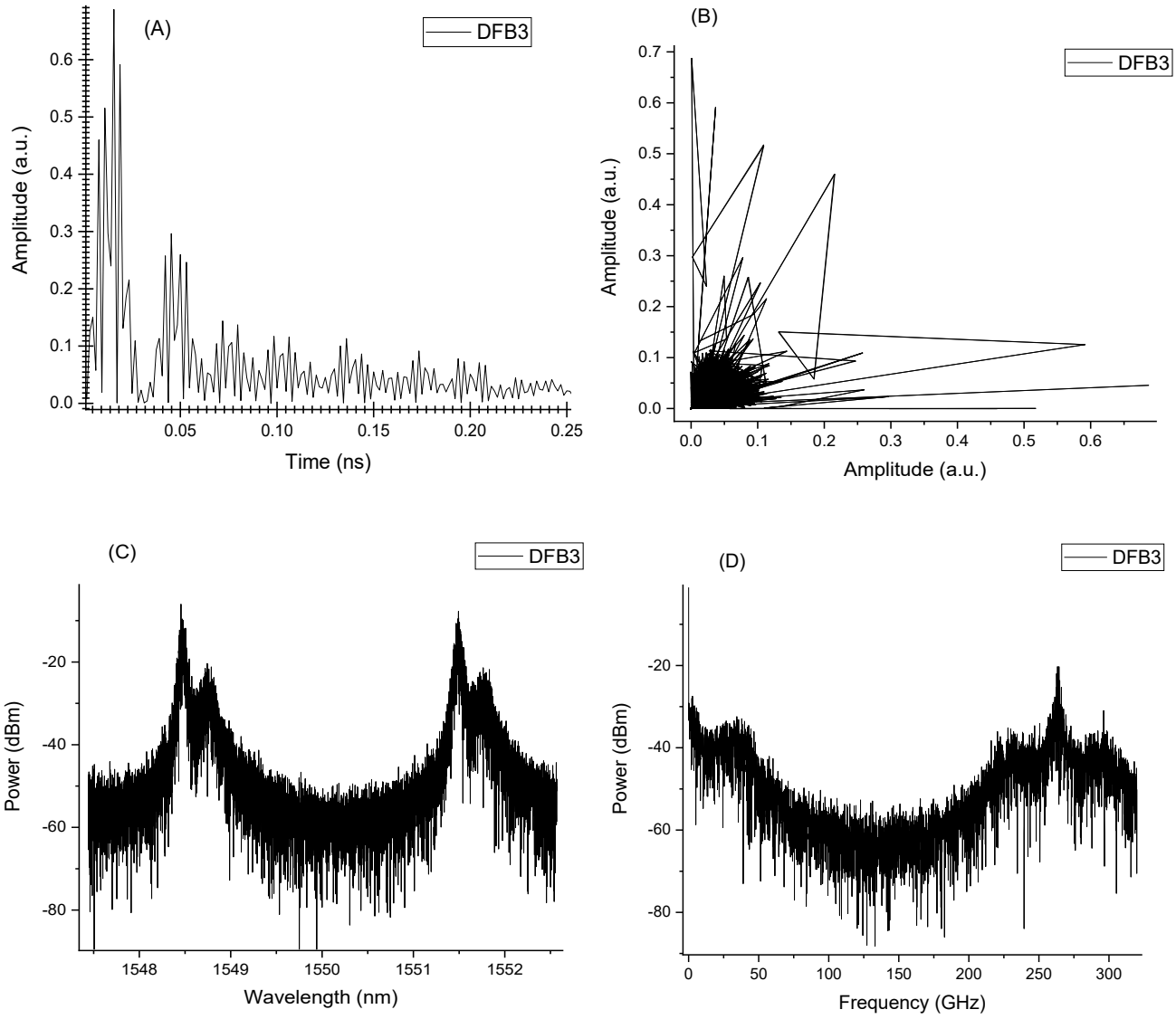

Fig. 6. Resulted spectrum of DFB3 of 20 dB gain of EDFA.
(A) Time series, (B) Phase space, (C) Optical spectrum and (D) Radio frequency spectrum

4.3. Loop dynamics with 50 dB gain

The effect of optical gain from EDFA, as reported in Table 1, directly affects the DFB2 and DFB3 laser sources shown in Fig. 1, more than the remaining laser sources in the loop. Such an effect is achieved via optical injection into DFB2 and via modulation in DFB3. Conventional gain is a ratio between output power and input power (equation 13). While power for the signal is increased, chaotic dynamics are also increased, as shown in Fig. 7 for all DFBs. Noting That phase shift value is selected to be 180 degrees.

4.3.1. DFB1 laser - multimode operation

DDB1 laser source is inserted after an UFBG, and the transmitted spectrum from this filter becomes an input for it. The results shown in Fig. 7(C, D) indicate generation for new neighbor modes directly behind the original modes, with defferent peaks. Based on the attractor, such new lasing peaks appeared as shown in Fig.7(A,B), and the route to chaos states was observed more than in the state of 20dB gain of amplifing.

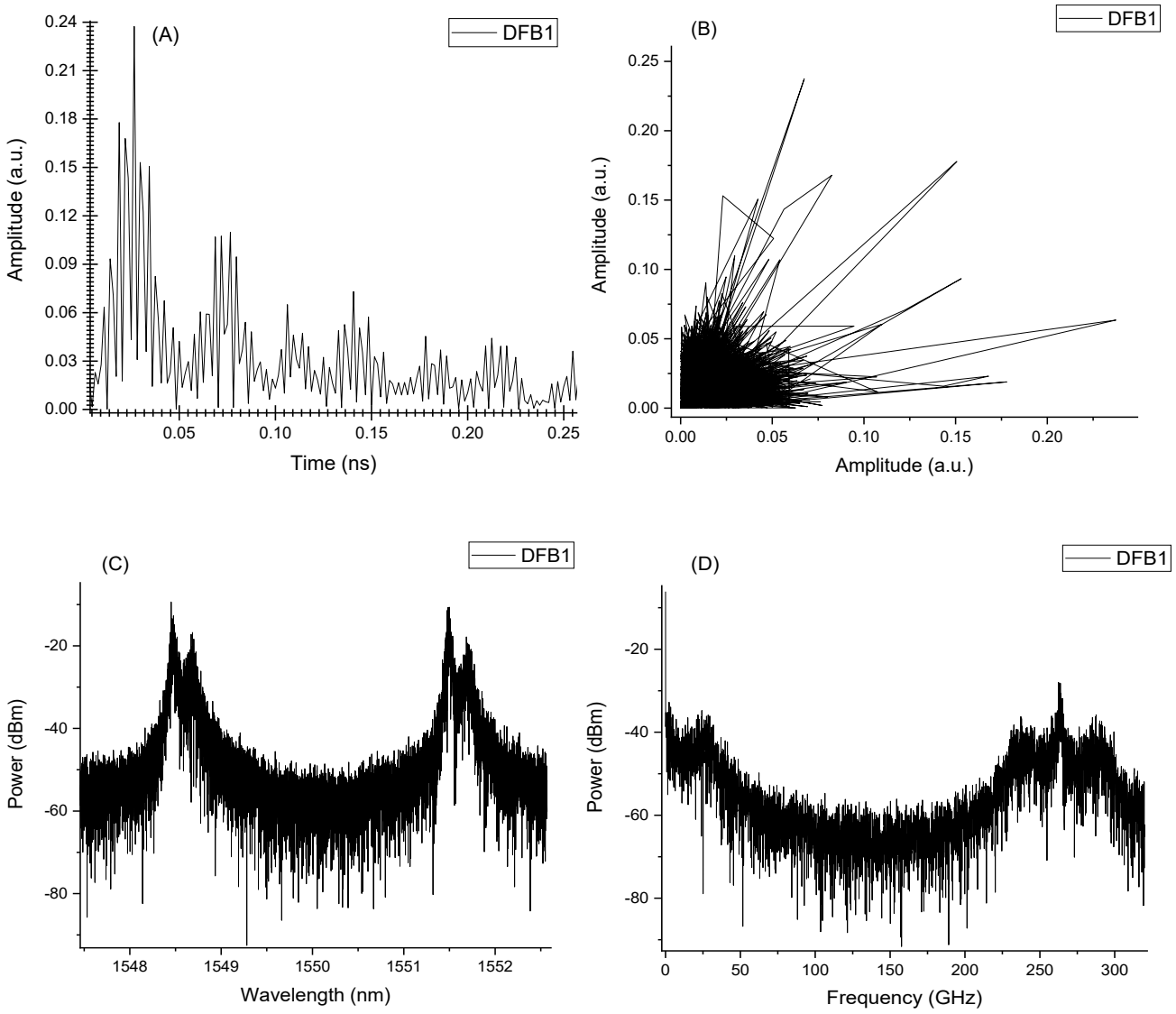

Fig. 7. Observed spectrum of DFB1 of 50 dB gain of EDFA.
(A) Time series, (B) Phase space, (C) Optical spectrum and (D) Radio frequency spectrum

4.3.2. DFB2 laser - multimode operation

DFB2 is inserted in the reflected port from the UFBG and amplifying gain increased to 50 dB; this makes spectrum changes and nonlinearity effect appeared as shown in Fig. 8. The chaotic behavior in time domain and attracter in Fig. 8 (A, B) investigated. This indicates a modification in the semiconductor active medium inside this laser source. Spikes are observed in the resulting spectrum, with different spacing between them indicating the interaction between different circulating modes.

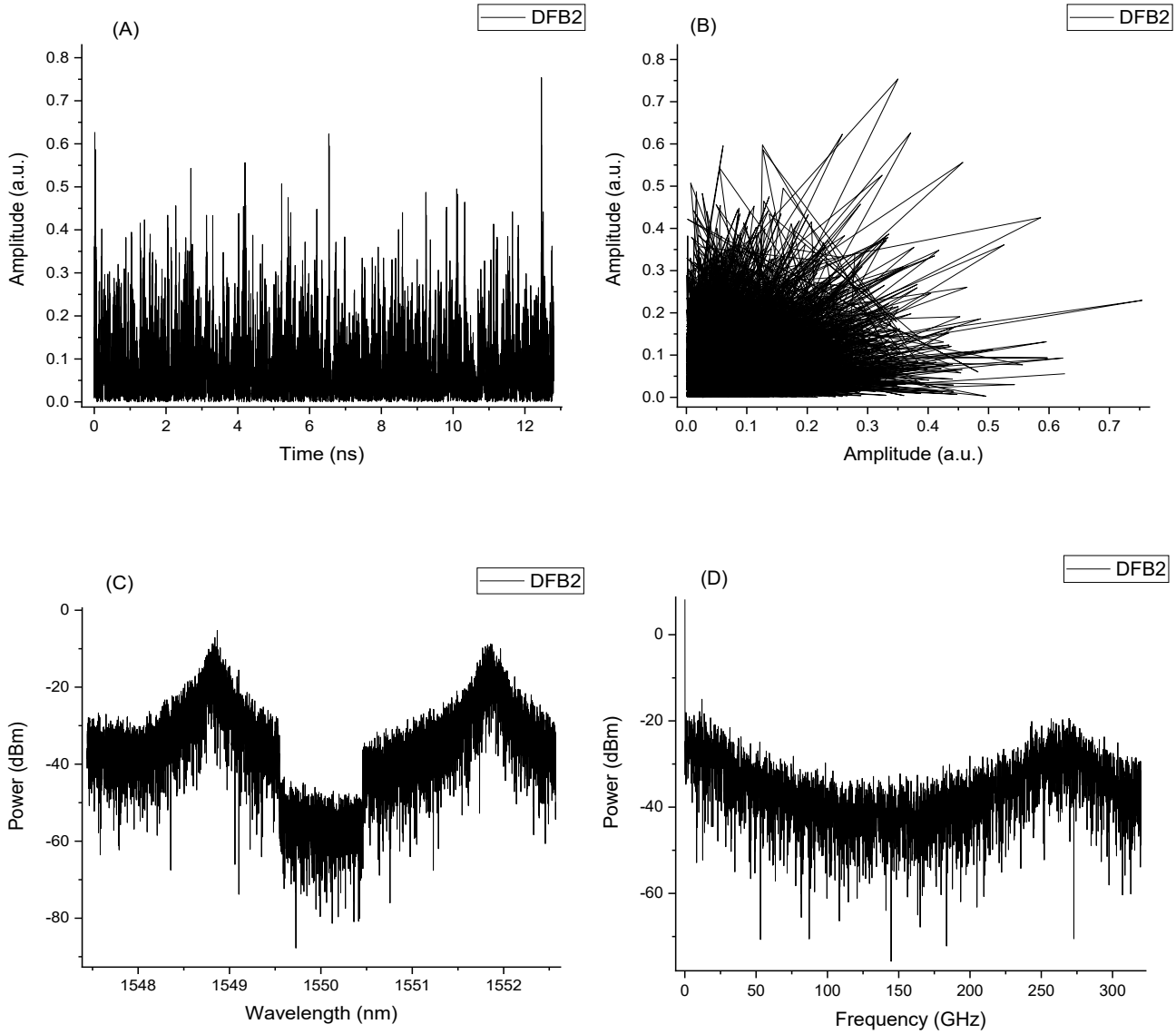

Fig. 8. Observed spectrum of DFB2 of 50 dB gain of EDFA.
(A) Time series, (B) Phase space, (C) Optical spectrum and (D) Radio frequency spectrum

4.3.3. DFB3 laser - multimode operation

DFB3 is inserted after the NOLM, which means the output of the loop becomes input of DFB3. The resulting spectrum is shown in Fig. 9. Several modes appeared more than those observed. A more complicated chaotic signal is resulted under the effect of an amplified circulated path inside the loop mirror.

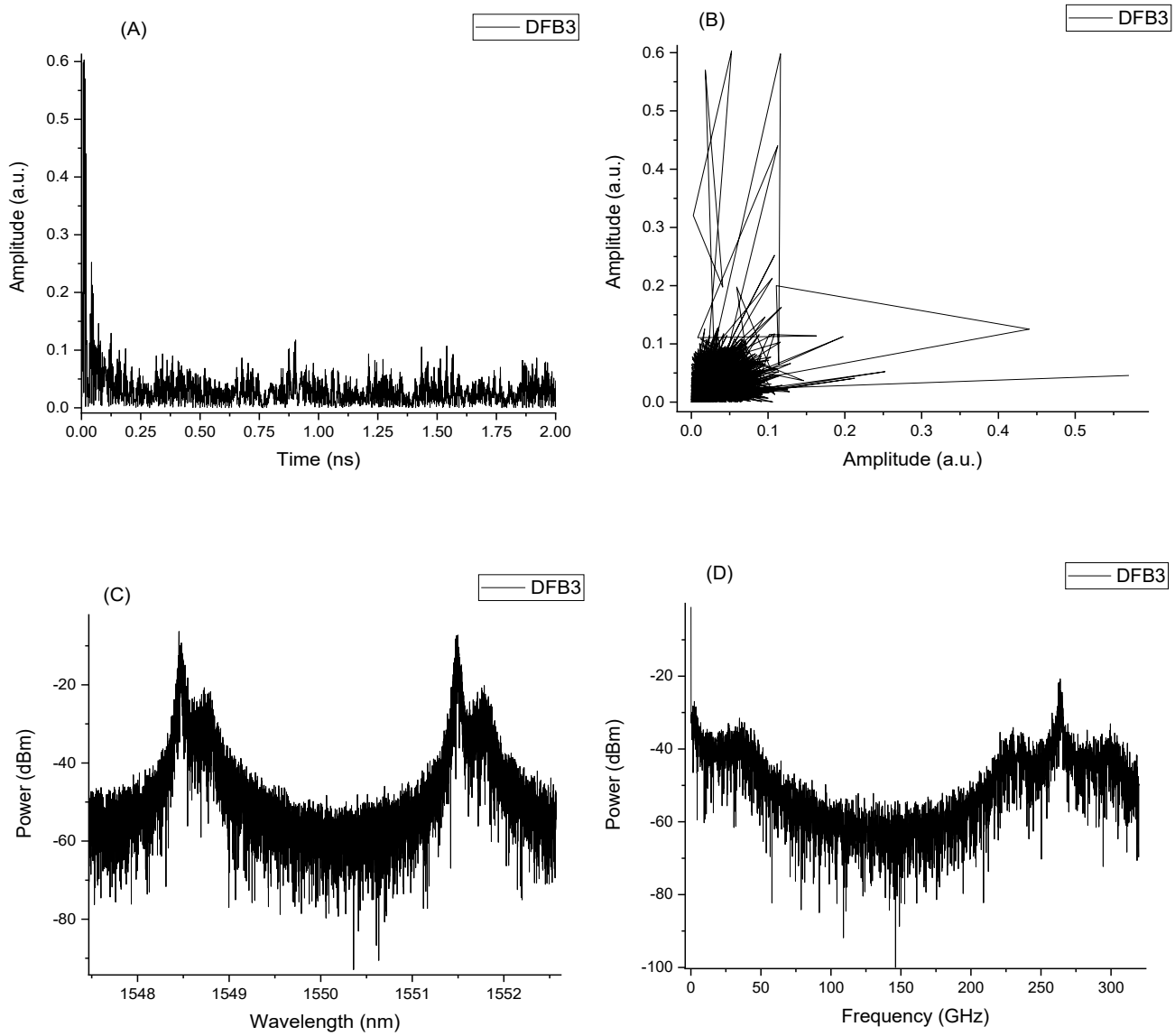

Fig. 9. Observed spectrum of DFB3 of 50 dB gain of EDFA.
(A) Time series, (B) Phase space, (C) Optical spectrum and (D) Radio frequency spectrum.

4.4 Loop dynamics with 80 dB gain

4.4.1. DFB1 laser- multimode operation

Switch to multi-mode selection from the software menu, and the laser source will operate in a different rate equation model. The insertion of noise-like signals will be more effective via the generation of two chaotic signals. Then, even with low disturbances, there is a chaotic signal due to a specific ratio of incoherent optical feedback and injection. Fig. 10 shows the resultant dynamics with this gain value.

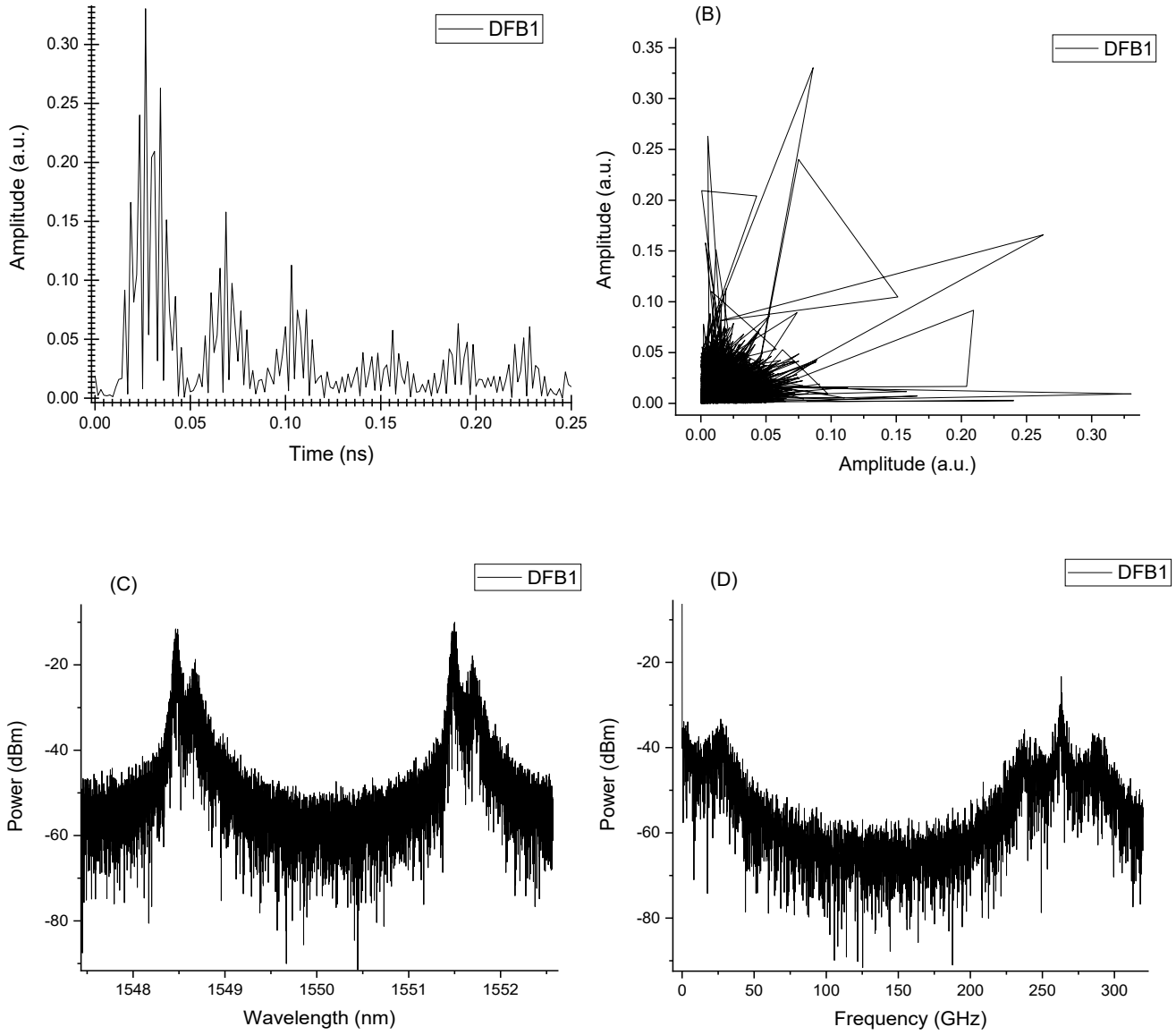

Fig. 10. Observed spectrum of DFB1 of 80 dB gain of EDFA.
(A) Time series, (B) Phase space, (C) Optical spectrum and (D) Radio frequency spectrum

4.4.2. DFB2 laser- multimode operation

In comparison with the results shown in Fig. 5, the spikes, shown in Fig. 11, become sharper and have higher amplitudes than those observed earlier. Spacing between them is also changed under the new interaction rules. The power spectrum and RF spectrum are widely different than those observed at lower gain values i.e. the elimination for Gaussian signal is observed, indicating the coherence collapse in this result.

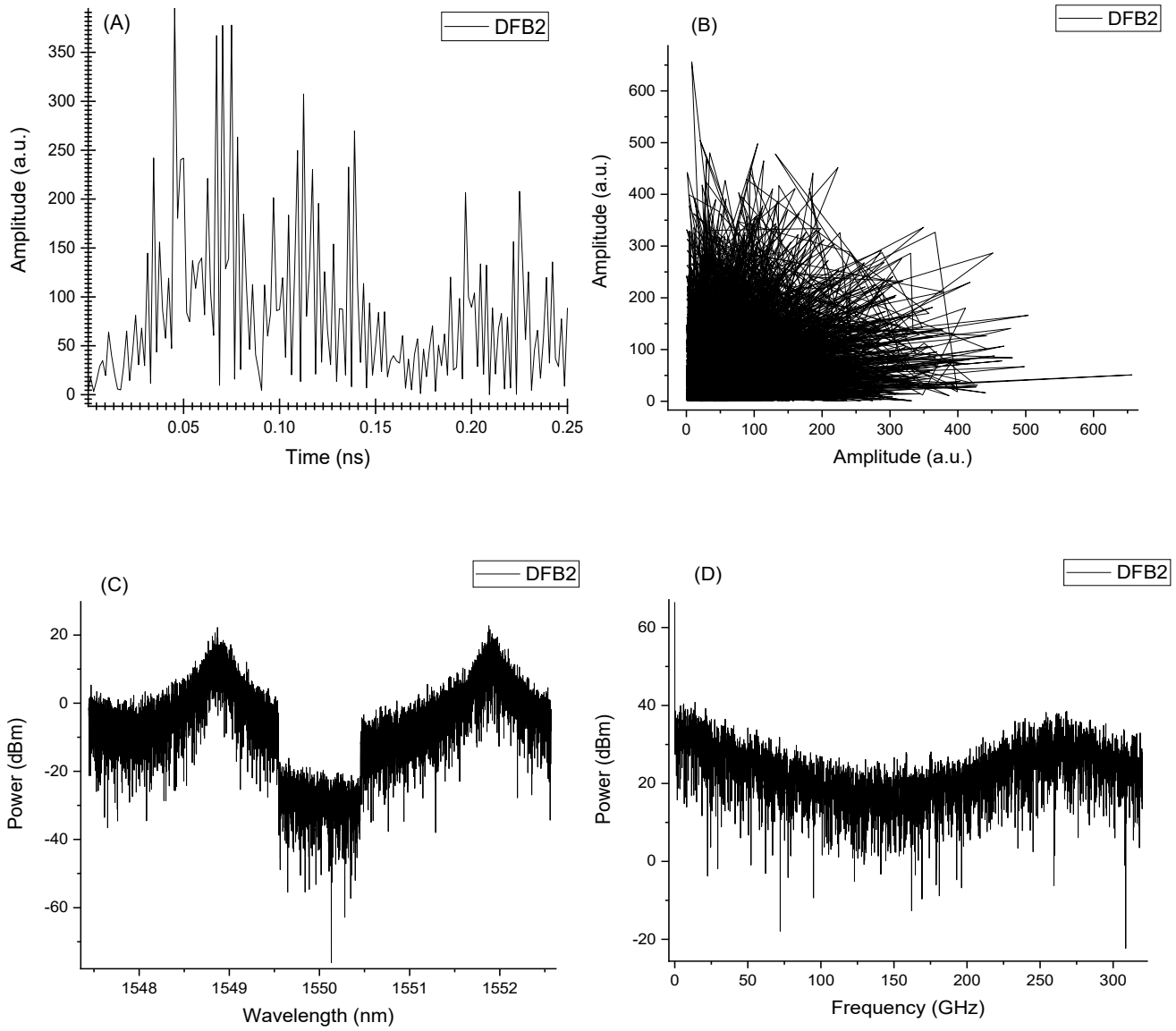

Fig. 11. Observed spectrum of DFB2 of 80 dB gain of EDFA.
(A) Time series, (B) Phase space, (C) Optical spectrum and (D) Radio frequency spectrum

4.4.3. Multimode DFB3 laser

As shown in Fig. 12, time series for this laser is includes more neighbor lasing modes. While the optical power spectrum and RF spectrum show support for the basic two modes originally observed in the first laser, i.e., lasers out of the mirror. More modes and nonlinearity increased with increased gain of amplifing through loop mirroras shown in Fig. 12 (C,D) for Time domian and`frequency domian. Coherence collapse in attracter spectrum can note in Fig. 12(B).

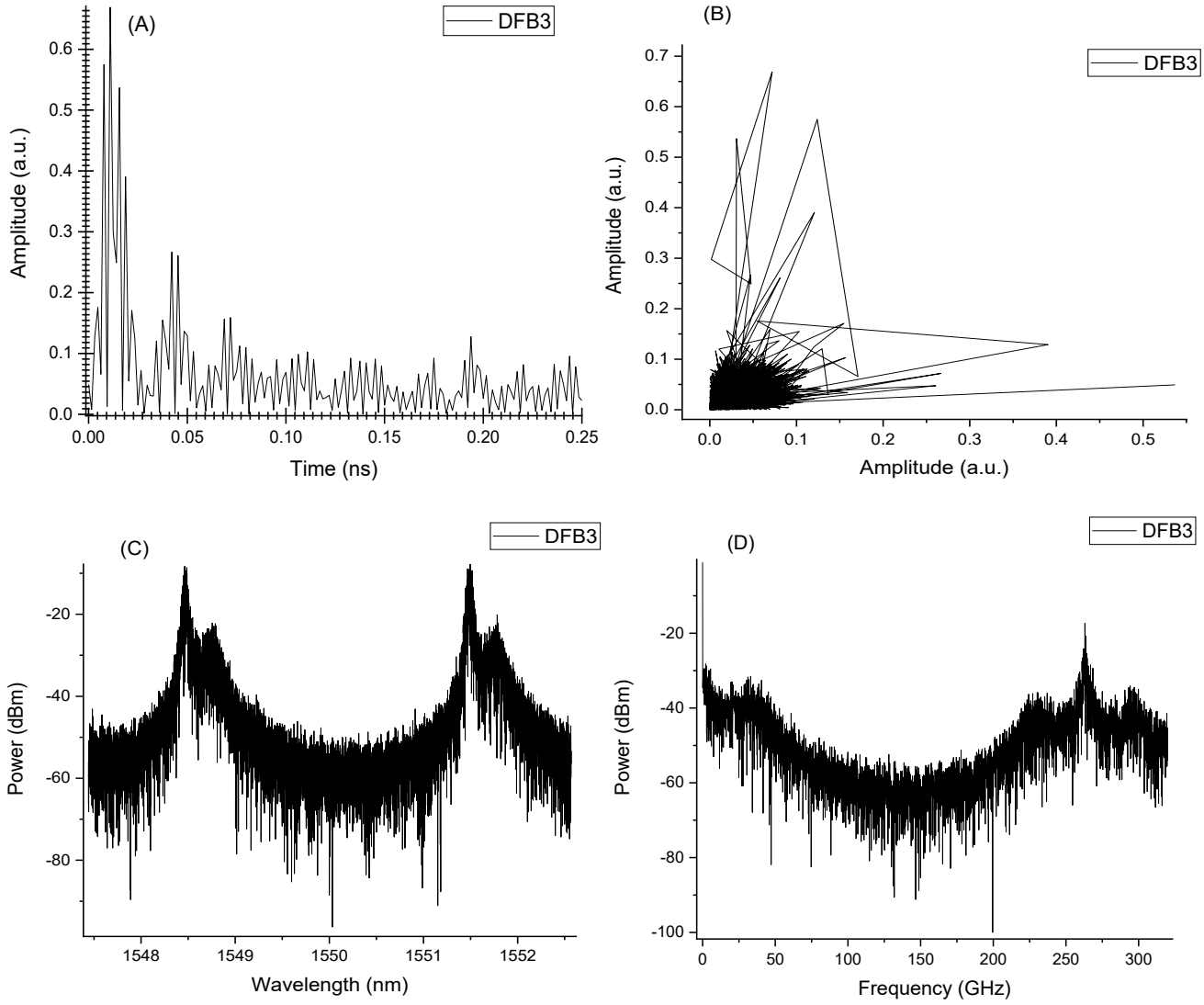

Fig. 12. Observed spectrum of DFB3 of 80 dB gain of EDFA.
(A) Time series, (B) Phase space, (C) Optical spectrum and (D) Radio frequency spectrum

5. Conclusion

Insertion of EDFA inside a nonlinear fiber loop mirror has desirable properties. Tested parameters such as phase, amplification, filteration, and current operation level were added to the chaotic dynamics introduced in this work. The optical feedback and injection inside this NOLM, in combination with filtering, led to the generation of chaotic signals. Coherence collapse was always attributable to deterministic chaos. In each case the proximate cause of coherence collapse was interaction between the optical injection through NOLM. Induced the achievement of several neighboring modes with high power and a chaotic signal is also observed. Strange or chaotic attractors are investigated. According to simulation demonstrations, mode competition is physically responsible for the low-frequency amplification in the multi-mode chaotic outputs.

References

[1] C.-X. Shi, Optics Communications **107**, 276 (1994).
[2] G. P. Agrawal, Applications of Nonlinear Fiber Optics, Academic Press, San Diego 2001.
[3] G. P. Agrawal, Fiber-Optic Communication Systems, John Wiley & Sons, New York 2002.
[4] T. Ch, Journal of Optoelectronics Engineering **2**(2), 29 (2014).
[5] A. M. Parekhan, R. O. Banaz, International Journal of Engineering, Mathematical and Physical Sciences **2**(10), 752 (2008).
[6] L. A. Ivan, D. V. Roman, F. A. Andrei, K. I. Sergey, Frontiers in Optics/Laser Science **21**(6), 1 (2016).
[7] R. G. Zainab, H. A. Ayser, Optoelectron. Adv. Mat. **16**(7-8), 307 (2022).
[8] A. A. Hemed, Chaos Generation Methods in Optical Communication Systems, Baghdad: University of Baghdad, 2011.

[9] R. E. Pidgeon, D. E. Frymyer, "Optical Amplifier Basic Properties And System Modeling: A Simple Tutorial," NCTA Technical Papers, Scientific-Atlanta, Inc., 1992.
[10] K. Remya, International Journal of Engineering and Technical Research (IJETR) **3**(8), 154 (2015).
[11] N. A. Nour, H. R. Muhammed, Y. A. Hassan, Muthanna Journal of Pure Science **7**(2), 39 (2020).
[12] A. W. Naji, B. A. Hamida, X. S. Cheng, M. A. Mahdi, S. Harun, S. Khan, W. F. AL-Khateeb, A. A. Zaidan, B. B. Zaidan, H. Ahmad, International Journal of the Physical Sciences **6**(20), 4674 (2011).
[13] T. Okoshi, Optical Amplifiers and Their Applications 1990, paper PDP11 (1990).
[14] P. E. Rezin, F. E. Don, "Optical Amplifier Basic Properties And System Modeling:," NCTA Technical Papers 86 1992.
[15] M. H. Adnan, H. A. Ayser, Journal University of Kerbala **15**(1), 40 (2017).
[16] M. Eiselt, W. Pieper, H. G. Weber, Journal of Lightwave Technology **13**(10), 2099 (1995).
[17] J. M. Senior, Optical Fiber Communications Principles and Practice, Hall Europe, 2009.
[18] A. A. Hemed, R. S. Abbas, COSTR-V8, Hooghly, West Bengal, India, BP International 120 (2022).
[19] A. A. Hemed, R. S. Abbas, The 8th International Conference on Applied Science and Technology (ICAST 2020) AIP Conference Proceedings **2290**, 050021 (2020), Karbala, Iraq, 2020.
[20] R. S. Abbas, A. A. Hemed, New Trends in Physical Science Research **5**, Hooghly, West Bengal, India, BP International 109 (2022).
[21] R. S. Abbas, A. A. Hemed, 1st Diyala International Conference for Pure and Applied Science: ICPAS2021. AIP Conference Proceedings **2593**, 020004 (2023), Diyala Iraq, 2023.
[22] G. P. Agrawal, N. K. Dutta, Semiconductor Lasers-Second Edition, USA: Kluwer Academic Publishers, 2001.
[23] C. L. Shun, Physics of Photonic Devices, 2nd Edition, OSA: Wiley Series in Pure and Applied Optics, 2008.
[24] W. Zheng, G. W. Taylor, IEEE Journal of Quantum Electronics **43**(4), 295 (2007).
[25] A. J. Lowery, IEE Proceedings **137**(5), 293 (1990).
[26] Y. Lingzhen, Z. Li, Y. Rong, Y. Li, Y. Baohua, Y. Ping, Optics Communications **285**, 143 (2012).
[27] A. A. Hemed, Z. R. Gaiab, **2022** International Conference on Computer Science and Software Engineering (CSASE), Duhok, Iraq 194 (2022).
[28] T. M. Prasanna, Study of all fiber optic current transducer in optical transmission system and evaluation of the performance onoptisystem, California: California State University Northridge, 2016.
[29] C. Cheng, X. Min, Elsevier, Optics Communications **254**, 215 (2005).
[30] L. Hua, Y. Jun, M. G. John, IEEE, Journal of Quantum Electronics **29**(9), 2421 (1993).

*Corresponding authors: mayads539@gmail.com
suhaalawsi@gmail.com